THE GEOLOGICAL SOCIETY OF AMERICA®

Carbonate platform production during the Cretaceous

Alexandre Pohl[1,2,3,†], Yannick Donnadieu[1], Yves Godderis[4], Cyprien Lanteaume[1,5,6], Alex Hairabian[7], Camille Frau[1], Julien Michel[1,5], Marie Laugie[1], John J.G. Reijmer[7], Christopher R. Scotese[8], and Jean Borgomano[1]

[1]*Aix Marseille Université, CNRS, IRD, Coll France, INRA, CEREGE, Aix-en-Provence, France*
[2]*Department of Earth Sciences, University of California, Riverside, California 92521, USA*
[3]*Biogéosciences, UMR 6282, UBFC/CNRS, Université Bourgogne Franche-Comté, 6 boulevard Gabriel, F-21000 Dijon, France*
[4]*UMR5563 Géosciences Environnement Toulouse, Observatoire Midi-Pyrénées, CNRS, Toulouse, France*
[5]*MODIS Pau, 4 rue Jules Ferry, Pau, France*
[6]*Total CSTJF, avenue Larribeau, 64000 Pau, France*
[7]*College of Petroleum Engineering & Geosciences, King Fahd University of Petroleum & Minerals, Dhahran 31261, Saudi Arabia*
[8]*Department of Earth & Planetary Sciences, Northwestern University, Evanston, Illinois 60201, USA*

ABSTRACT

Platform carbonates are among the most voluminous of Cretaceous deposits. The production of carbonate platforms fluctuated through time. Yet, the reasons for these fluctuations are not well understood, and the underlying mechanisms remain largely unconstrained. Here we document the long-term trend in Cretaceous carbonate platform preservation based on a new data compilation and use a climate-carbon cycle model to explore the drivers of carbonate platform production during the Cretaceous. We show that neritic carbonate preservation rates followed a unimodal pattern during the Cretaceous and reached maximum values during the mid-Cretaceous (Albian, 110 Ma). Coupled climate-carbon cycle modeling reveals that this maximum in carbonate deposition results from a unique combination of high volcanic degassing rates and widespread shallow-marine environments that served as a substrate for neritic carbonate deposition. Our experiments demonstrate that the unimodal pattern in neritic carbonate accumulation agrees well with most of the volcanic degassing scenarios for the Cretaceous. Our results suggest that the first-order temporal evolution of neritic carbonate production during the Cretaceous reflects changes in continental configuration and volcanic degassing. Geodynamics, by modulating accommodation space, and turnovers in the dominant biota probably played a role as well, but it is not necessary to account for the latter processes to explain the first-order trend in Cretaceous neritic carbonate accumulation in our simulations.

INTRODUCTION

In recent years, our knowledge of the geological evolution of the surficial carbon cycle has greatly improved. Among the main advances is the reconstruction of the Phanerozoic atmospheric CO_2 (Berner, 2006; Foster et al., 2017). The fluctuations of the carbon sink due to continental weathering as well as the change in solid Earth degassing have been at least partly constrained using models (Goddéris et al., 2014; Brune et al., 2017) or proxies (such as isotopes) (Veizer et al., 1999; Cao et al., 2017). One major component of the carbon cycle, however, the sedimentary carbonate sink, has been poorly investigated at the global scale. Many data have been published regarding carbonate accumulation fluxes (Bosscher and Schlager, 1993; Kiessling et al., 2000), but data compilations and extrapolation at the global scale are scarce.

Carbonate sediments are the receptacles of the atmospheric CO_2 that has been removed from the atmosphere by weathering and can be subsequently recycled along subduction zones (Mason et al., 2017; Pall et al., 2018). Carbonate sediment deposition thus reflects many coupled processes. Identifying those processes through geological time is an unparalleled way to check whether we have understood the overall functioning of the carbon cycle or not.

Here we investigate the production of carbonate platforms during the Cretaceous, one of the most prolific periods of carbonate platform development (Kiessling et al., 2003). We reconstruct temporal variations in platform carbonate deposition based on a new data compilation and subsequently explore the drivers of the temporal trends in Cretaceous carbonate production using a coupled climate-carbon cycle model.

METHODS

Database of Shallow-Water Carbonate Preservation Rates

We compiled, from published studies, an extensive database of Cretaceous shallow-water marine carbonate preservation rates (see the GSA Data Repository for the full database[1]). The latter were calculated by dividing the estimated sediment thickness by the stratigraphic interval duration. Calculated preservation rates necessarily underestimate actual carbonate production rates. Indeed, neritic carbonate accumulation is limited by depositional accommodation space. In addition, deposits may subsequently undergo dissolution, erosion, and compaction, and produced sediments may be exported toward the basin. As a result of all those mechanisms acting to reduce the thickness of the carbonates preserved on the shelves, preservation rates calculated based on the geological record are typically one to several orders of magnitude lower than production rates

Alexandre Pohl http://orcid.org/0000-0003-2328-351X

[†]alexpohl@ucr.edu.

[1]GSA Data Repository item 2020192, supplementary information, geological database, experimental setup and climate model runs (Sections S1–S2, Figs. S1–S2, and Tables S1–S2), is available at http://www.geosociety.org/datarepository/2020 or by request to editing@geosociety.org.

 https://doi.org/10.1130/B35680.1; 3 figures; Data Repository item 2020192.

measured on present-day, carbonate-secreting ecosytems such as coral reefs (Bosscher, 1992; Strasser and Samankassou, 2003; Schlager, 2010). Therefore, compiled preservation rates are considered to significantly underestimate the actual accumulation rates. Considering the multiple mechanisms acting to reduce the thickness of the shallow-water carbonates preserved on the shelves, maximum preservation rates are further considered to be the most representative of the original carbonate accumulation flux in ancient times.

The GEOCLIM Climate-Carbon Cycle Model

We used the GEOCLIM climate-carbon cycle model (see footnote 1) to simulate carbonate accumulation fluxes during the Cretaceous. The GEOCLIM model (Donnadieu et al., 2006a) asynchronously couples a carbon cycle box model with a general circulation model and represents a significant improvement over the zero-dimensional GEOCARB-like models (Berner, 2006), since continental weathering rates are resolved spatially, taking into account the continental configuration and sea level (Goddéris et al., 2014). The carbon cycle box model is the COMBINE model upgraded following Donnadieu et al. (2006a) and includes a robust representation of the marine sub-cycles of inorganic and organic carbon, oxygen, alkalinity, and phosphorus. The model explicitly represents the spatial distribution of silicate, basalt, and carbonate weathering as a function of climate. The oceans are modeled by nine "boxes." The accumulation of neritic carbonates takes place exclusively in the box representing the low- to mid-latitude epicontinental photic zone, following equation 1:

$$F = k_{cr} \times A_{platform} \times (\Omega_{ara} - 1)^{1.7}. \quad (1)$$

where F is the neritic carbonate depositional flux (mol yr^{-1}), $A_{platform}$ is the shelf area available to shallow-water carbonate deposition derived from the paleogeographic reconstructions, Ω_{ara} is the model aragonite solubility ratio, and k_{cr} is a calibration constant. This formulation of neritic carbonate accumulation rates has been successfully used in previous studies to investigate the consequences of the demise of carbonate platforms during the Middle–Late Jurassic transition (ca. 160 Ma; Donnadieu et al., 2011) and the effects of the breakup of Pangea on neritic carbonate accumulation (Late Permian to Late Cretaceous; Donnadieu et al., 2006a). The climatic component of GEOCLIM is the FOAM ocean-atmosphere model version 1.5 (Jacob, 1997), a mixed-resolution general circulation model that has been routinely used to study climate in deep time, including during the Cretaceous (Donnadieu et al., 2006b; Ladant and Donnadieu, 2016).

Simulations were conducted using the Cretaceous paleogeographical reconstructions of Scotese (2016) and Scotese and Wright (2018) with deep-ocean bathymetry after Müller et al. (2008). Changing solar luminosity values were modeled after the stellar physics of Gough (1981). Earth's orbit around the Sun was circular (null eccentricity), and the obliquity was set to 22°. This orbital configuration provides an equal, annual insolation for both hemispheres with minimal seasonal contrast.

RESULTS

Temporal Variations in Cretaceous Shallow-Water Carbonate Preservation Rates

At first order, Figure 1 shows a unimodal pattern in neritic carbonate preservation rates during the Cretaceous with background values <70 m $m.y.^{-1}$ and an excursion to higher preservation rates up to 175–200 m $m.y.^{-1}$ during the mid-Cretaceous between 125 Ma (Aptian) and 95 Ma (Cenomanian). This mid-Cretaceous maximum is a robust feature and was highlighted by the previous Phanerozoic compilation of Bosscher and Schlager (1993). It parallels the mid-Cretaceous local maximum in reefal carbonate production identified by Kiessling et al. (2000) and also corresponds with the development of massive successions of sediments in the Mediterranean Tethys (>100 m thick; Skelton and Gili, 2012) and with the maximum in carbonate accumulation identified in the North American, Russian, and Siberian platforms (Whitten, 1976).

Coupled Climate-Carbon Cycle Simulations

The drivers of secular change in platform carbonate production have been the subject of investigation for decades (Schlager, 1981; Bosscher and Schlager, 1993; Kiessling et al., 2000; Donnadieu et al., 2006a). From a carbon cycle perspective, global carbonate deposition is tightly linked to changes in continental silicate and carbonate weathering. However, several factors impact the distribution of carbonate deposition between the open ocean and shallow-marine platforms. Debate thus continues as to whether fluctuations in neritic carbonate accumulation rates reflect changing environmental conditions such as global climate and evolving geodynamics (e.g., continental configuration and subsidence) or intrinsic changes such as turnovers in dominant biota, since different carbonate factories are known to be associated with different carbonate production rates (e.g., Lanteaume et al., 2018). Previous attempts to identify these complex relationships over the course of the Phanerozoic failed to reach any definitive conclusions (Bosscher and Schlager, 1993; Kiessling et al., 2000).

Baseline Simulations with Present-Day Volcanism

We used the GEOCLIM climate-carbon cycle model (Donnadieu et al., 2006a) to investigate the driving mechanisms for the Cretaceous trend in neritic carbonate deposition with a special focus on the maximum in carbonate accumulation centered at 110 Ma (see Fig. 1). Simulations were run every 10 m.y. between 150 Ma (Late Jurassic) and 60 Ma (Paleocene). For each time slice and associated continental configuration, the GEOCLIM model computed the pCO_2 value by balancing volcanic degassing

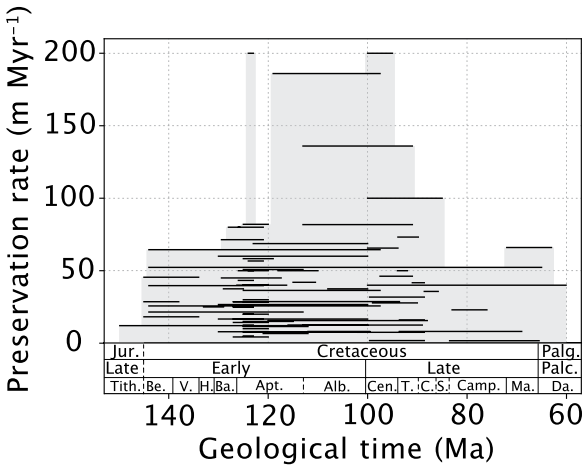

Figure 1. Compilation of Cretaceous neritic carbonate preservation rates. The light gray envelope represents the maximum accumulation rates, which are likely to best represent neritic carbonate production in ancient times (see Methods). Stratigraphic boundaries after Gradstein et al. (2012). Alb.—Albian; Apt.—Aptian; Ba.—Barremian; Be.—Berriasian; Camp.—Campanian; Cen.—Cenomanian; C.—Coniacian; Da.—Danian; H.—Hauterivian; Jur.—Jurassic; Ma.—Maastrichtian; Palc.—Paleocene; Palg.—Paleogene; S.—Santonian; T.—Turonian; Tith.—Tithonian; V.—Valanginian.

with silicate weathering. The GEOCLIM model simulated the associated climatic state and ocean biogeochemistry. Though the neritic carbonate deposition rate was focus of our investigation, the simulated pCO_2 was used to evaluate the fit of our simulations to the latest pCO_2 reconstruction of Foster et al. (2017). The latter criterion was chosen to compare our simulations to proxy data due to the critical role that pCO_2 plays on ocean pH and thus carbonate geochemistry.

In our baseline runs, the rate of volcanic degassing was set to the present-day value (6.8×10^{12} moles of carbon per year; Donnadieu et al., 2006a) (Fig. 2A); only the paleogeography and associated climate varied from one time slice to another. Simulated pCO_2 was lower than indicated by the proxy compilation for most of the Cretaceous (Fig. 2B). Yet, an interesting pattern emerged: the bimodal trend observed in the pCO_2 compilation between 120 Ma and 60 Ma (gray shading in Fig. 2B) was well reproduced in the baseline runs (black line in Fig. 2B). This suggests that the temporal variations in pCO_2 reconstructed by Foster et al. (2017) between 120 Ma and 60 Ma may be largely due to the paleogeographical evolution. The total neritic carbonate depositional flux simulated in the baseline runs varied very little between 150 Ma and 60 Ma, showing only a local optimum at 80 Ma (Fig. 2C).

Numerical Simulations Using Cretaceous Volcanic Degassing Scenarios

As a second step, we used Cretaceous plate models and data compilations to derive volcanic CO_2 degassing scenarios, which could help reconcile the simulations with proxy-based pCO_2 reconstructions. Such modeling attempts face limitations due to the large uncertainties in reconstructing Cretaceous volcanic degassing. Indeed, numerous studies have been published that attempt to reconstruct one of the components of the degassing rate, but there is no reconstruction of the total CO_2 degassing by the solid Earth at the geological timescale. The lack of an integrated curve requires us to rely on incomplete reconstructions. Such bias concerns both the modeling and data communities. For instance, McKenzie et al. (2016) argue for a dominant role of degassing on the climatic evolution, based on a correlation between the Phanerozoic climate and their curve for the degassing of arc volcanism, although arc volcanism is only one component of the total degassing.

The rationale that we adopted thus consists of using available constraints to compute total volcanic degassing rates, expressed as ratios compared to the present-day value. We did not try to identify the individual contributions of the different components: subduction zones, rifts, mid-ocean ridges, and arc volcanism. Instead, we followed the approach adopted by Berner in his various versions of the seminal GEOCARB(SULF) model (Berner and Kothavala, 2001; Berner, 2004, 2006), which consists of scaling volcanic degassing with proxies for geodynamic activity (e.g., subduction length). Although this approach will undoubtedly benefit soon from advances in geodynamic models, it has been shown to produce very good results in the GEOCARB model (Berner, 2006; Van Der Meer et al., 2014). In detail, we derived volcanic degassing rates (Fig. 2A) from the lengths of subduction zones calculated by Van Der Meer et al. (2014) (hereafter VDM14), from the area of subducted lithosphere reconstructed over the last 180 m.y. by Engebretson et al. (1992) (E92), from the slab flux estimated by East et al. (2020) (EA20), and from the continental arc activity compiled by Cao et al. (2017) (CAO17). We also used the C1' and C1'' scenarios of Brune et al. (2017), which consider variable contributions of rifts, mid-ocean ridges, subduction zones, and continental arcs.

Our model does not account for the degassing from large igneous provinces (LIPs). LIP degassing has been shown to increase the atmospheric partial pressure of CO_2 for durations that do not exceed a few million years after the end of the onset (Dessert et al., 2001). LIPs also impact the carbonate system through short-term acidification of the ocean just prior to the response of the weathering system (Paris et al., 2016). However, here we explore the response of the carbon cycle to processes acting at a longer timescale, on the order of 10 m.y.

We tested each of the volcanic degassing scenarios in the GEOCLIM model. The best fit to

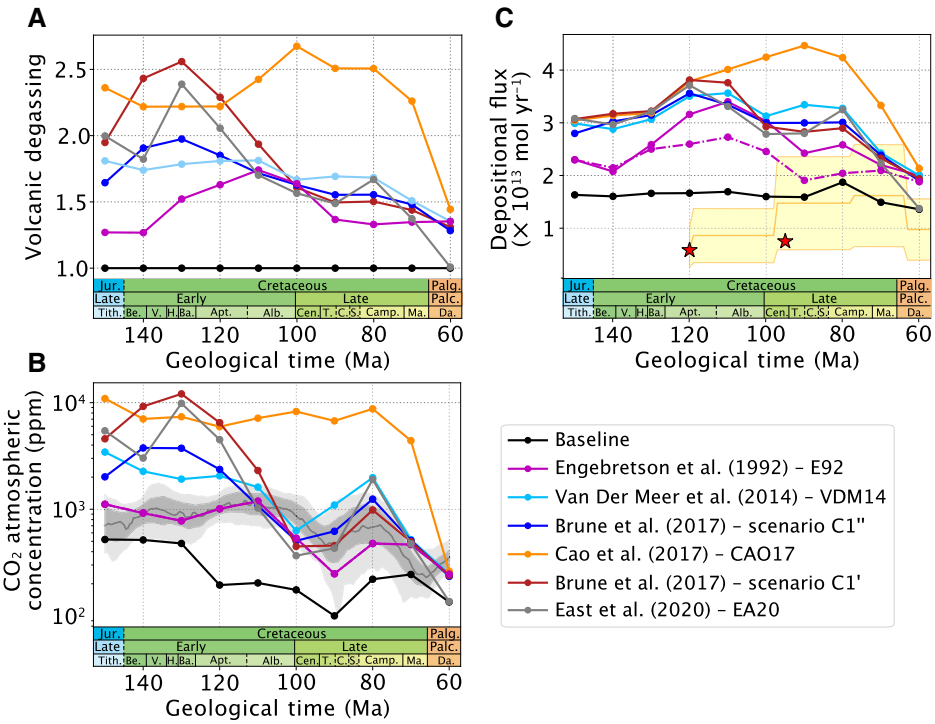

Figure 2. Model results for (A) volcanic degassing scenarios used in the GEOCLIM model (ratio to present-day value), (B) predicted atmospheric CO_2 concentration, and (C) predicted neritic carbonate total depositional flux. Black line represents the baseline runs with volcanic degassing set to the present-day level. Solid color lines represent volcanic degassing scenarios. For scenario E92, the simulation represented with the dashed line is identical to the one represented with the solid line except that it uses a constant area of the shallow-marine environments available to neritic carbonate deposition during the Cretaceous. In panel B, background gray shading represents the proxy-based pCO_2 reconstruction of Foster et al. (2017) with LOESS fit, 68% and 95% confidence intervals. In panel C, yellow shading and red stars, respectively, represent the platform carbonate accumulation fluxes estimated by Dutkiewicz et al. (2019) and Skelton (2003) (see text). Alb.—Albian; Apt.—Aptian; Ba.—Barremian; Be.—Berriasian; Camp.—Campanian; Cen.—Cenomanian; C.—Coniacian; Da.—Danian; H.—Hauterivian; Jur.—Jurassic; Ma.—Maastrichtian; Palc.—Paleocene; Palg.—Paleogene; S.—Santonian; T.—Turonian; Tith.—Tithonian; V.—Valanginian.

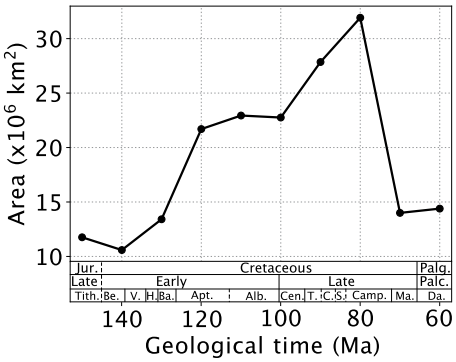

Figure 3. Area of the shallow-marine environments available to neritic carbonate deposition, derived from the paleogeographical reconstructions (see footnote 1). Alb.—Albian; Apt.—Aptian; Ba.—Barremian; Be.—Berriasian; Camp.—Campanian; Cen.—Cenomanian; C.—Coniacian; Da.—Danian; H.—Hauterivian; Jur.—Jurassic; Ma.—Maastrichtian; Palc.—Paleocene; Palg.—Paleogene; S.—Santonian; T.—Turonian; Tith.—Tithonian; V.—Valanginian.

proxy data was obtained using the subduction-based degassing scenario E92 (Fig. 2B). The neritic carbonate production flux associated with this best-guess scenario displayed a maximum centered on 110 Ma (Fig. 2C) that agreed well with our compilation of Cretaceous preservation rates (see Fig. 1).

Analyzing the Drivers of the Mid-Cretaceous Maximum in Carbonate Accumulation

Despite the disparities in the volcanic degassing scenarios (Fig. 2A), most simulations showed that the highest rates of neritic carbonate production occurred during the mid-Cretaceous (between ca. 120 Ma and 80 Ma). The mid-Cretaceous unimodal pattern, bounded by an increase in neritic carbonate production in the Early Cretaceous (120–130 Ma) and a decrease in neritic carbonate production in the early Late Cretaceous (80 Ma), was a robust pattern that was shared by different degassing scenarios.

Comparison of the simulations that considered evolving volcanic degassing rates with the baseline runs (color vs. black lines in Fig. 2C) revealed that the lowest to mid-Cretaceous increase in neritic carbonate production (130–120 Ma), at least partially, relied on an increase in volcanic degassing rates. In addition, a sensitivity test that used a constant area of the neritic environments available for carbonate deposition (dashed, magenta line in Fig. 2C) demonstrated that the latter area played a key role in the increase in shallow-marine carbonate production. Indeed, the area of the continental shelves significantly rose between 130 Ma and 120 Ma in our reconstructions (Fig. 3). This increase resulted from the strong eustatic rise that took place at that time (Müller et al., 2008). In the E92 scenario, the increasing area of shallow-marine environments strengthened the pattern of carbonate accumulation already imposed by changing volcanism (Fig. 2C) by favoring the accumulation of carbonate in neritic environments at the expense of the open ocean. In other degassing scenarios that did not have a well-defined maximum at 120–110 Ma (i.e., C1', C1'', VDM14, CAO17, EA20), the increasing area of the shallow-marine environments, alone, drove the increase in neritic carbonate production between 130 Ma and 120 Ma (Figs. 2A and 2C). Regarding the decrease in carbonate production after 80 Ma, two main mechanisms were in play; most scenarios showed a drop in volcanic degassing (Fig. 2A), and a major eustatic fall (Müller et al., 2008) reduced the area of the shallow-marine environments available to neritic carbonate deposition (Fig. 3).

DISCUSSION

Comparison of our simulated trend of shallow-water carbonate production with the updated compilation of preservation rates allowed us to propose a mechanistic explanation for temporal variations in the deposition of Cretaceous shallow-water carbonates. It would be even more interesting and straightforward to compare our simulated fluxes with the volumes (instead of vertical aggradation rates) of shallow-water carbonates produced during the Cretaceous. Unfortunately, such comparison is hampered by the lack of robust quantification of these volumes. For instance, Dutkiewicz et al. (2019) calculated platform carbonate accumulation fluxes by multiplying the extent of the carbonate platforms mapped by Kiessling et al. (2003) by globally uniform preservation rates derived from the compilation of Bosscher and Schlager (1993). Figure 1C reveals that the temporal trends of carbonate production simulated in GEOCLIM and the preserved volumes reconstructed by Dutkiewicz et al. (2019) largely differ. The estimates of Dutkiewicz et al. (2019) provide significantly lower values. The low values at least partly reflect the action of dissolution, erosion, compaction, and the export of the carbonates toward the basin, which all tend to reduce the thickness of the carbonates deposited on the shelves. Preserved volumes necessarily represent an underestimation of the volume of carbonate that is actually produced (see Methods). Regarding the temporal trend, the reconstruction of Dutkiewicz et al. (2019) does not provide any robust quantification of the variation in the production of platform carbonates. Indeed, the approach of Dutkiewicz et al. (2019) consists of multiplying the surface of the carbonate platforms documented in the geological database by a constant (i.e., a uniform rate of vertical aggradation). The authors derived two values for this constant rate from the compilation of Bosscher and Schlager (1993), which provided the lower (using 30 m m.y.$^{-1}$) and upper (using 80 m m.y.$^{-1}$) boundaries for their reconstructed trend (Fig. 1C). Our updated compilation of preservation rates (Fig. 1), however, reveals that preservation rates cover a very large range of values, from <10 m m.y.$^{-1}$ to 200 m m.y.$^{-1}$. While the approach employed by Dutkiewicz et al. (2019) probably reflects the best estimate that can be produced at the global scale based on current knowledge, it neglects the spatio-temporal variations in carbonate accumulation rates and thus exclusively reflects the evolution of the area of the carbonate platforms (compare Fig. 1C and Fig. 3). Skelton (2003) conducted similar calculations for the Aptian and Cenomanian. Only the platforms of the Tethyan region were considered in these calculations, while Dutkiewicz et al. (2019) considered the area of the platforms at the global scale. The fact that both studies led to virtually identical values (Fig. 1C), although they focused on significantly different spatial scales, highlights once again the difficulty in estimating the depositional flux by neritic carbonates in deep time. We argue that, considering the current difficulty of estimating volumes of neritic carbonates produced in ancient times, our reconstructed neritic carbonate preservation rates (Fig. 1) constitute an instructive proxy for the efficiency of the shallow-water carbonate factory in ancient times. The reported temporal patterns are supported by both previous data compilations (Whitten, 1976; Bosscher and Schlager, 1993; Kiessling et al., 2000) and accumulation patterns observed in the field (Skelton and Gili, 2012).

CONCLUSION

The simulated maximum in mid-Cretaceous neritic carbonate production results from the combination of high volcanic degassing levels and the large shallow-marine realms. Although the precise evolution of carbonate accumulation rates varies from one volcanic degassing scenario to another, the unimodal pattern in neritic carbonate production simulated during the Cretaceous is robust and shows up in most of the scenarios. The model results align well with the temporal trend that emerges from the updated compilation of Cretaceous platform carbonate preservation rates. Our results therefore suggest that the first-order evolution of neritic carbonate deposition during the Cretaceous reflects changes in continental configuration and volcanic

degassing. Other mechanisms modulating accommodation space and turnovers in the dominant biota probably played a role as well, but our simulations suggest that the latter processes do not explain the first-order trend in Cretaceous neritic carbonate accumulation.

ACKNOWLEDGMENTS

The authors thank Dietmar Müller, Peter Skelton, and two anonymous reviewers for thorough reviews that significantly strengthened the manuscript, and Rob Strachan, Judith Totman Parrish, and Gerald Dickens for editorial handling. Alexandre Pohl and Yannick Donnadieu thank the Commissariat à l'énergie atomique et aux énergies alternatives, Centre de Calcul Recherche et Technologie for providing access to the high-performance computing resources of Très Grand Centre de Calcul under the allocation 2014-012212 made by GENCI. This project has received funding from the European Union's Horizon 2020 research and innovation programme under the Marie Sklodowska-Curie grant agreement no. 838373. This work reflects only the author's view; the European Agency is not responsible for any use that may be made of the information in contains. The authors thank B. Suchéras-Marx (CEREGE) for interesting discussions on calcifying plankton during the Cretaceous, P. Maffre (Géosciences Environnement Toulouse) for his assistance in setting up our Cretaceous configuration of the GEOCLIM model, and S. Brune for providing degassing scenarios.

REFERENCES CITED

Berner, R.A., 2004, The Phanerozoic Carbon Cycle: CO_2 and O_2: New York, Oxford University Press, 158 p.

Berner, R.A., 2006, GEOCARBSULF: A combined model for Phanerozoic atmospheric O_2 and CO_2: Geochimica et Cosmochimica Acta, v. 70, p. 5653–5664, https://doi.org/10.1016/j.gca.2005.11.032.

Berner, R.A., and Kothavala, Z., 2001, GEOCARB III: A revised model of atmospheric CO_2 over Phanerozoic time: American Journal of Science, v. 301, p. 182–204, https://doi.org/10.2475/ajs.301.2.182.

Bosscher, H., 1992, Growth potential of coral reefs and carbonate platforms [Ph.D. thesis]: Amsterdam, The Netherlands, Vrije Universiteit Amsterdam, 157 p.

Bosscher, H., and Schlager, W., 1993, Accumulation rates of carbonate platforms: The Journal of Geology, v. 101, p. 345–355, https://doi.org/10.1086/648228.

Brune, S., Williams, S.E., and Müller, R.D., 2017, Potential links between continental rifting, CO_2 degassing and climate change through time: Nature Geoscience, v. 10, p. 941–946, https://doi.org/10.1038/s41561-017-0003-6.

Cao, W., Lee, C.-T.A., and Lackey, J.S., 2017, Episodic nature of continental arc activity since 750 Ma: A global compilation: Earth and Planetary Science Letters, v. 461, p. 85–95, https://doi.org/10.1016/j.epsl.2016.12.044.

Dessert, C., Dupré, B., François, L.M., Schott, J., Gaillardet, J., Chakrapani, G., and Bajpai, S., 2001, Erosion of Deccan Traps determined by river geochemistry: Impact on the global climate and the $^{87}Sr/^{86}Sr$ ratio of seawater: Earth and Planetary Science Letters, v. 188, p. 459–474, https://doi.org/10.1016/S0012-821X(01)00317-X.

Donnadieu, Y., Goddéris, Y., Pierrehumbert, R., Dromart, G., Fluteau, F., and Jacob, R., 2006a, A GEOCLIM simulation of climatic and biogeochemical consequences of Pangea breakup: Geochemistry, Geophysics, Geosystems, v. 7, https://doi.org/10.1029/2006GC001278.

Donnadieu, Y., Pierrehumbert, R., Jacob, R., and Fluteau, F., 2006b, Modelling the primary control of paleogeography on Cretaceous climate: Earth and Planetary Science Letters, v. 248, p. 426–437, https://doi.org/10.1016/j.epsl.2006.06.007.

Donnadieu, Y., Dromart, G., Goddéris, Y., Pucéat, E., Brigaud, B., Dera, G., Dumas, C., and Olivier, N., 2011, A mechanism for brief glacial episodes in the Mesozoic greenhouse: Paleoceanography, v. 26, https://doi.org/10.1029/2010PA002100.

Dutkiewicz, A., Müller, M.D., Cannon, J., Vaughan, S., and Zahirovic, S., 2019, Sequestration and subduction of deep-sea carbonate in the global ocean since the Early Cretaceous: Geology, v. 47, p. 91–94, https://doi.org/10.1130/G45424.1.

East, M., Müller, R.D., Williams, S., Zahirovic, S., and Heine, C., 2020, Subduction history reveals Cretaceous slab superflux as a possible cause for the mid-Cretaceous plume pulse and superswell events: Gondwana Research, v. 79, p. 125–139, https://doi.org/10.1016/j.gr.2019.09.001.

Engebretson, D.C., Kelley, K.P., Cashman, H.J., and Richards, M.A., 1992, 180 Million years of subduction: GSA Today, v. 2, no. 5, p. 93–100.

Foster, G.L., Royer, D.L., and Lunt, D.J., 2017, Future climate forcing potentially without precedent in the last 420 million years: Nature Communications, v. 8, p. 14845, https://doi.org/10.1038/ncomms14845.

Goddéris, Y., Donnadieu, Y., Le Hir, G., Lefebvre, V., and Nardin, E., 2014, The role of palaeogeography in the Phanerozoic history of atmospheric CO_2 and climate: Earth-Science Reviews, v. 128, p. 122–138, https://doi.org/10.1016/j.earscirev.2013.11.004.

Gough, D.O., 1981, Solar interior structure and luminosity variations: Solar Physics, v. 74, p. 21–34, https://doi.org/10.1007/BF00151270.

Gradstein, F.M., Ogg, J.G., Schmitz, M., and Ogg, G., eds., 2012, The Geologic Time Scale, Volumes 1 & 2: Elsevier Science, 1176 p.

Jacob, R.L., 1997, Low frequency variability in a simulated atmosphere-ocean system [Ph.D. thesis]: Madison, University of Wisconsin, 170 p.

Kiessling, W., Flügel, E., and Golonka, J., 2000, Fluctuations in the carbonate production of Phanerozoic reefs, *in* Insalaco, E., et al., eds., Carbonate Platform Systems: Components and Interactions: Geological Society, London, Special Publication 178, p. 191–215, https://doi.org/10.1144/GSL.SP.2000.178.01.13.

Kiessling, W., Flügel, E., and Golonka, J., 2003, Patterns of phanerozoic carbonate platform sedimentation: Lethaia, v. 36, p. 195–226, https://doi.org/10.1080/00241160310004648.

Ladant, J.-B., and Donnadieu, Y., 2016, Palaeogeographic regulation of glacial events during the Cretaceous supergreenhouse: Nature Communications, v. 7, no. 12771, https://doi.org/10.1038/ncomms12771.

Lanteaume, C., Fournier, F., Pellerin, M., and Borgomano, J., 2018, Testing geologic assumptions and scenarios in carbonate exploration: Insights from integrated stratigraphic, diagenetic, and seismic forward modeling: The Leading Edge, v. 37, p. 672–680, https://doi.org/10.1190/tle37090672.1.

Mason, E., Edmonds, M., and Turchyn, A.V., 2017, Remobilization of crustal carbon may dominate volcanic arc emissions: Science, v. 357, p. 290–294, https://doi.org/10.1126/science.aan5049.

McKenzie, N.R., Horton, B.K., Loomis, S.E., Stockli, D.F., Planavsky, N.J., and Lee, C.-T.A., 2016, Continental arc volcanism as the principal driver of icehouse-greenhouse variability: Science, v. 352, p. 444–447, https://doi.org/10.1126/science.aad5787.

Müller, R.D., Sdrolias, M., Gaina, C., Steinberger, B., and Heine, C., 2008, Long-term sea-level fluctuations driven by ocean basin dynamics: Science, v. 319, p. 1357–1362, https://doi.org/10.1126/science.1151540.

Pall, J., Zahirovic, S., Doss, S., Hassan, R., Matthews, K.J., Cannon, J., Gurnis, M., Moresi, L., Lenardic, A., and Dietmar Müller, R., 2018, The influence of carbonate platform interactions with subduction zone volcanism on palaeo-atmospheric CO_2 since the Devonian: Climate of the Past, v. 14, p. 857–870, https://doi.org/10.5194/cp-14-857-2018.

Paris, G., Donnadieu, Y., Beaumont, V., Fluteau, F., and Goddéris, Y., 2016, Geochemical consequences of intense pulse-like degassing during the onset of the Central Atlantic Magmatic Province: Palaeogeography, Palaeoclimatology, Palaeoecology, v. 441, p. 74–82, https://doi.org/10.1016/j.palaeo.2015.04.011.

Schlager, W., 1981, The paradox of drowned reefs and carbonate platforms: Geological Society of America Bulletin, v. 92, p. 197–211, https://doi.org/10.1130/0016-7606(1981)92<197:TPODRA>2.0.CO;2.

Schlager, W., 2010, Ordered hierarchy versus scale invariance in sequence stratigraphy: International Journal of Earth Sciences, v. 99, p. 139–151, https://doi.org/10.1007/s00531-009-0491-8.

Scotese, C.R., 2016, PALEOMAP PaleoAtlas for GPlates and the PaleoData Plotter Program: PALEOMAP Project, 2016, https://www.earthbyte.org/paleomap-paleoatlas-for-gplates/.

Scotese, C.R., and Wright, N., 2018, PALEOMAP Paleodigital Elevation Models (PaleoDEMS) for the Phanerozoic: PALEOMAP Project, 2018, https://www.earthbyte.org/paleodem-resource-scotese-and-wright-2018/.

Skelton, P.W., 2003, The operation of the major geological carbon sinks, *in* Skelton, P.W., Spicer, R.A., Kelley, S.P., and Gilmour, I. eds., The Cretaceous World: Cambridge, England, Cambridge University Press, p. 259–266.

Skelton, P.W., and Gili, E., 2012, Rudists and carbonate platforms in the Aptian: A case study on biotic interactions with ocean chemistry and climate: Sedimentology, v. 59, p. 81–117, https://doi.org/10.1111/j.1365-3091.2011.01292.x.

Strasser, A., and Samankassou, E., 2003, Carbonate sedimentation rates today and in the past: Holocene of Florida Bay, Bahamas, and Bermuda vs. Upper Jurassic and lower Cretaceous of the Jura Mountains (Switzerland and France): Geologia Croatica, v. 56, p. 1–18, https://doi.org/10.4154/GC.2003.01.

Van Der Meer, D.G., Zeebe, R.E., Van Hinsbergen, D.J.J., Sluijs, A., Spakman, W., and Torsvik, T.H., 2014, Plate tectonic controls on atmospheric CO_2 levels since the Triassic: Proceedings of the National Academy of Sciences of the United States of America, v. 111, no. 12, p. 4380–4385, https://doi.org/10.1073/pnas.1315657111.

Veizer, J., et al., 1999, $^{87}Sr/^{86}Sr$, $\delta^{13}C$ and $\delta^{18}O$ evolution of Phanerozoic seawater: Chemical Geology, v. 161, p. 59–88, https://doi.org/10.1016/S0009-2541(99)00081-9.

Whitten, E.H.T., 1976, Cretaceous phases of rapid sediment accumulation, continental shelf, eastern USA: Geology, v. 4, p. 237–240, https://doi.org/10.1130/0091-7613(1976)4<237:CPORSA>2.0.CO;2.

Science Editor: Rob Strachan

Manuscript Received 28 February 2020
Manuscript Accepted 16 March 2020

Printed in the USA